培地で3時間インキュベーションし、その後培地を糖無添加の培地に変えて、さらに 48 時間 10%FBS 含有培地でインキュベーションして、その後分泌されたルシフェラーゼ発現量をピカジーンを用いて測定した。

凍結乾燥再水和法調製リポソーム製剤による遺伝子導入実験

MHAPC と DOPE 脂質がモル比で 1:1 のリポソーム（MHAPC-Lip）、または、MHAPC と DOPE とバイオ界面活性剤 MEL-A がモル比で 1:1:0.5 のリポソーム(MEL-A-MHAPC-Lip)を薄膜法で調製し、ルシフェラーゼをコードしたプラスミド DNA pCMV-luc を用いて、(+/-)荷電比 3/1 の複合体を調製した。この懸濁液に全脂質の5倍質量のシュクロース、またはマルトースを添加した懸濁液（A）と、その凍結乾燥製剤（B）と、それを再水和した懸濁液（C）を用いて、A549 細胞、またはマウスに気管内投与をして遺伝子導入効率を調べた。なお、(C)は 1.55 mg 粉末を 60 μl 水で再水和した(333 ng DNA/ml)。凍結乾燥再水和前リポソームのサイズは、約 200 nm であり、凍結乾燥再水和後は約 1-5 μm であった。

遺伝子導入効率は、A, C 懸濁液を1ウエルあたり 2 μg DNA となるように添加して、24 時間 10%FBS 含有培地でインキュベーションし、ルシフェラーゼ発現量を測定した。B では、3.1 mg (40 μg DNA 含有)の凍結乾燥製剤をマウスの気管に内径 5 μm の注射針の注射筒を用いて肺に投与した。

遺伝子導ナノ粒子製剤の細胞毒性

遺伝子発現時の各細胞の毒性は、WST8 測定から評価した。

C．研究結果

ナノ粒子/DNA の遺伝子導入効率に対する糖の影響

ナノ粒子/DNA は細胞培地に各糖を添加して、2種類の細胞で遺伝子導入効率を調べた (Fig. 1)。どちらの細胞においても、シュクロースの添加時に最も高い遺伝子発現が見られ、マルトース、トレハロース、ラクトースでは遺伝子発現の低下が見られた。このときの細胞毒性は各糖類で顕著な差が見られなかったことにより、遺伝子発現の差は細胞への導入効率の差によると推察された。

また、シュクロースの添加において，複合体形成時の塩の影響を調べたところ、10～50mM NaCl でさらに発現が高くなることが明らかになった (Fig. 2)。

遺伝子導入リポソーム製剤へ糖の影響

MHAPC-Lip、MEL-A-MHAPC-Lip/DNA 複合体とマルトース，またはシュクロースを添加した懸濁液A、または、その凍結乾燥再水和液Cと細胞とインキュベーションした結果、MEL-A-MHAPC-Lip にシュクロースを添加した系では、凍結乾燥前 A に比べて約１０倍高い遺伝子導入効率を示した(Fig. 3)。さらに、この凍結乾燥製剤 B をマウスに気管内投与して、肺での遺伝子導入効率を調べたが、十分な発現はみられなかった。

D．考察

遺伝子導入用リポソームベクターでは、Tg の低いシュクロースを添加して凍結乾燥再水和時すると遺伝子導入効率が高くなり、糖はリポソームの安定性よりも DNA の局所の安定性に寄与している可能性があることを報告した[1]。

もし、糖が DNA の局所の安定性に寄与しているならば、リポソームでなく、ナノ粒子によっても同じように遺伝子導入効率が上昇するはずである。そこで、本研究は、５種類の２糖がナノ粒子/DNA の遺伝子導入効率に及ぼす影響について調べた。その結果、リポソームの凍結乾燥再水和時と同様に、シュクロースの培地への添加によって遺伝子導入効率が高くなった。この結果より，シュクロースは複合体中の DNA や、複合体の分散性などに大きな影響を与えることが示唆された。また、複合体形成時の塩濃度が遺伝子導入効率に大きく寄与することも明らかとなった。シュクロースは、複合体中の DNA と局所的な水素結合等の相互作用によって安定性に寄与している可能性が示

唆された。

シュクロースを添加した凍結乾燥再水和法で調製した遺伝子封入リポソーム製剤をマウスの肺に投与して遺伝子導入効率を調べた結果、十分な発現を得ることはできなかった。これはリポソームのサイズが１ミクロン以上と大きくなったために、粘膜透過性が低下したためと推察された。

E．結論

本研究の結果より、in vivo 用遺伝子導入用製剤には、リポソーム/DNA 複合体のサイズの制御が重要であることが明らかとなった。今後，糖添加量の最適化を行う。

F．健康危険情報

なし

G．研究発表

1．論文発表

1) Y. Maitani , Y. Aso , A. Yamada, S. Yoshioka. Effect of sugars on storage stability of lyophilized liposome /DNA complexes with high transfection efficiency, *Int. J. Pharm.*, in press.

2) A. Hayama, T. Yamamoto, M. Yokoyama, K. Kawano, Y. Hattori, Y. Maitani. Polymeric micelles modified by folate-PEG-lipid for targeted drug delivery to cancer cells in vitro. *J. Nanosci. Nanotechnol.*, in press

3) M. Furuhata, R. Danev, K. Nagayama, Y. Yamada, H. Kawakami, K. Toma, Y. Hattori, Y. Maitani. Decaarginine-PEG-artificial lipid/DNA complex for gene delivery: nanostructure and transfection efficiency, *J. Nanosci. Nanotechnol.*, in press.

4) N. Takahashi, Y. Watanabe, Y. Maitani, T. Yamauchi, K. Higashiyama, T. Ohba. p-Dodecylaminophenol derived from the synthetic retinoid, fenretinide: Antitumor efficacy in vitro and in vivo against human prostate cancer and mechanism of action. *Int. J. Cancer,* in press

5) H.L .Ma, X.R. Qi, W.X. Ding, Y. Maitani, T. Nagai. Magnetic targeting after femoral artery administration and biocompatibility assessment of superparamagnetic iron oxide nanoparticles. *J. Biomed. Mater. Res. A.* (2007) in press.

6) W. Ding, Y. Hattori, Y. Maitani. Hydroxyethylated cationic cholesterol derivatives in liposome vectors promote gene expression in the lung. *Int. J. Pharm.*, accepted.

7) M. Fukushima, Y. Hattori, H. Tsukada, K. Koga, E. Kajiwara, K. Kawano, T. Kobayashi, K. Kamata, Y. Maitani. Adiponectin gene therapy of streptozotocin-induced diabetic mice using hydrodynamic injection. *J. Gene Med.*, 9: 976-985 (2007)

8) Y. Hattori, Y. Maitani. Low-molecular-weight polyethylenimine enhanced gene transfer by cationic cholesterol-based nanoparticle vector, *Biol. Pharm. Bull.*, 30(9) 1773-1778 (2007)

9) Y. Maitani, S. Igarashi, M. Sato, Y. Hattori. Cationic liposome (DC-Chol/DOPE＝1:2) and a modified ethanol injection method to prepare liposomes, increased gene expression, *Int. J. Pharm.*, 342: 33-39 (2007)

10) Y. Hattori, W. Ding, Y. Maitani. Highly efficient cationic hydroxyethylated cholesterol-based nanoparticle-mediated gene transfer in vivo and in vitro in prostate carcinoma PC-3 cells, *J. Control. Release*, 120: 122-130 (2007)

11) E. Kajiwara, K. Kawano, Y. Hattori, M. Fukushima, K. Hayashi, Y. Maitani. Long-circulating liposome-encapsulated ganciclovir enhances the efficacy of HSV-TK suicide gene therapy, *J. Control. Release,* 120: 104-110 (2007)

12) Y. Hattori, M. Fukushima and Y. Maitani. Non-viral delivery of connexin 43 gene with histone deacetylase inhibitor to human nasopharyngeal tumor cells enhances gene expression and inhibits in vivo tumor growth, *Int. J. Oncol.*, 30: 1427- 1439 (2007)

13) Y. Zhang, X.R. Qi, Y. Gao, L. Wei. Y. Maitani, T. Nagai. Mechanisms of co-modified liver-targeting liposomes as gene delivery carriers

based on cellular uptake and antigens inhibition effect. *J. Control. Release,* 117: 281-290 (2007)
14) Y. Hattori and Y. Maitani, DNA/lipid complex incorporated with fibronectin to cell adhesion enhances transfection efficiency in prostate cancer cells and xenografts. *Biol. Pharm. Bull.* 30: 603-607 (2007)
15) M. Fukushima, Y. Hattori, T. Yoshizawa, Y. Maitani. Combination of non-viral connexin 43 gene therapy and docetaxel inhibits the growth of human prostate cancer in mice. *International Journal of Oncology.* 30:225-231 (2007)

2. 学会発表

1) 羽山明宏、山本竜広、横山昌幸、川野久美、米谷芳枝、カンプトテシン封入高分子ミセルへの新規葉酸修飾法の検討と in vivo 評価、日本薬学会第 127 年会、2007.3.28-30
2) 山田敦史、川野久美、服部喜之、米谷芳枝、ドキソルビシン封入葉酸修飾リポソームの抗腫瘍効果における PEG 脂質の影響、日本薬学会第 127 年会、2007.3.28-30
3) 吉澤隆、服部喜之、米谷芳枝、葉酸受容体選択性 siRNA 遺伝子ベクターの開発、日本薬学会第 127 年会、2007.3.28-30
4) 藤田尭志、古幡昌彦、服部喜之、川上宏子、戸澗一孔、米谷芳枝、In vivo 用オリゴアルギニン脂質ベクターの開発、日本薬学会第 127 年会、2007.3.28-30
5) 服部喜之、丁武孝、米谷芳枝、正電荷コレステロールナノ粒子を用いた前立腺癌への遺伝子導入、日本薬剤学会第 22 年会、2007.5.21-23
6) 古幡昌彦、川上宏子、戸澗一孔、服部喜之、米谷芳枝、オリゴアルギニンミセル/DNA 複合体の構造と遺伝子導入効率、日本薬剤学会第 22 年会、2007.5.21-23
7) 丁武孝、服部喜之、東山公男、米谷芳枝、Cationic Cholesterol Derivatives for Gene Delivery into the Lung、日本薬剤学会第 22 年会、2007.5.21-23
8) 施力、服部喜之、川野久美、米谷芳枝、CPT-11 封入 PEG 修飾リポソームとカルボキシエステラーゼの腫瘍内補充による SN38 濃度の変化、日本薬剤学会第 22 年会、2007.5.21-23
9) 小野瀬絵里、川野久美、服部喜之、米谷芳枝、ミトキサントロン封入葉酸修飾リポソームの膜流動性と抗腫瘍効果、日本薬剤学会第 22 年会、2007.5.21-23
10) 服部喜之、米谷芳枝、正電荷コレステロールナノ粒子による plasmidDNA と短鎖 2 本鎖 RNA の前立腺癌への遺伝子導入、第 23 回日本 DDS 学会、2007.6.14-15
11) 山田敦史、阿曽幸雄、吉岡澄江、米谷、芳枝凍結乾燥再水和調製法による遺伝子封入リポソーム製剤の安定性に対する糖の影響、第 23 回日本 DDS 学会、2007.6.14-15
12) 日置敦子、川野久美、服部喜之、米谷芳枝、血中滞留性リポソームの in vitro 放出性評価、第 51 回日本薬学会関東支部大会、2007.10.6
13) 勢子祐貴、羽山明宏、山本竜広、横山昌幸、小野瀬絵里、川野久美、服部喜之、米谷芳枝、新規葉酸修飾カンプトテシン封入高分子ミセルの体内分布と抗腫瘍効果、第 51 回日本薬学会関東支部大会、2007.10.6
14) 古賀公子、服部喜之、米谷芳枝、悪性内分泌腫瘍の RET を標的とした siRNA による遺伝子治療、第 51 回日本薬学会関東支部大会、2007.10.6
15) 萩原彩子、服部喜之、米谷芳枝、癌細胞への siRNA 送達用脂質ナノ粒子の開発、第 51 回日本薬学会関東支部大会、2007.10.6

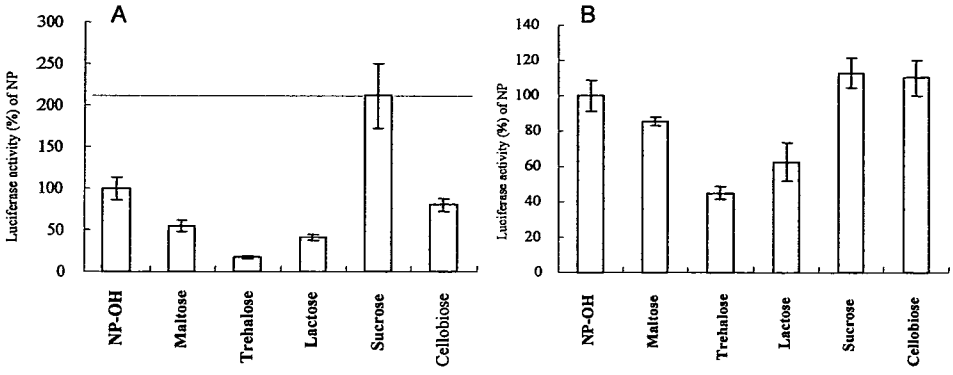

Fig. 1 Effect of sugars in medium on gene expression of nanoparticle (NP-OH) vector in PC-3(A) and SKBr3 (B) cells

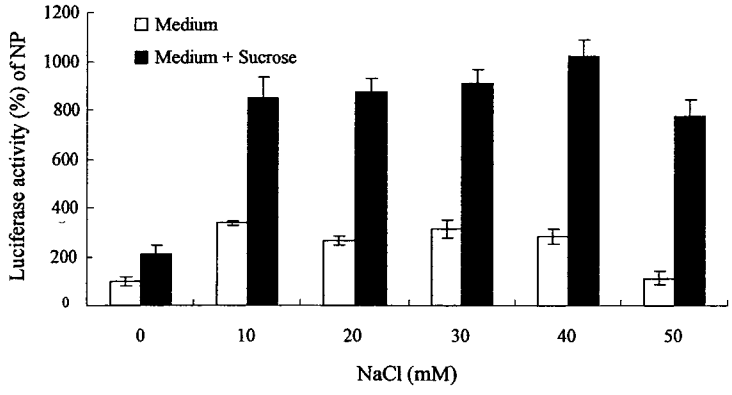

Fig. 2 Effect of NaCl concentration in medium with sucrose on gene expression of nanoparticle (NP-OH) vector in L1210 cells

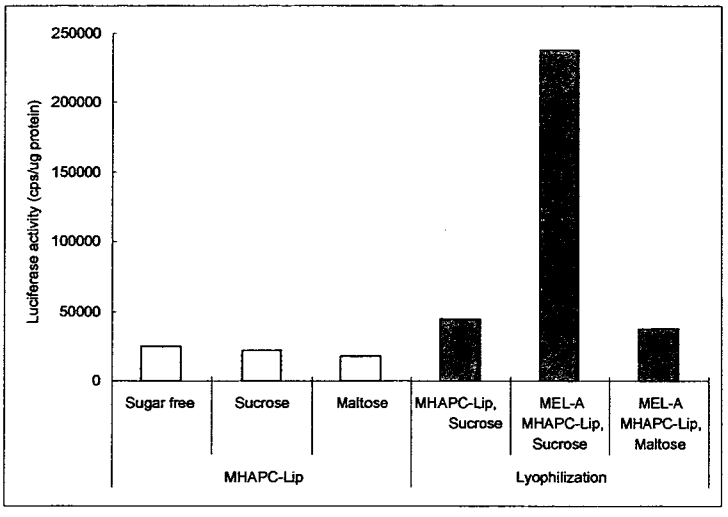

Fig. 3 Effect of sugars on gene expression of liposome and rehydration of lyophilized liposome vectors in A549 cells

別添５

研究成果の刊行に関する一覧表

雑誌

発表者氏名	論文タイトル名	発表誌名	巻号	ページ	出版年
Yoshioka, S., Aso, Y., Kawanishi, T	Wide-Ranging Molecular Mobilities of Water in Active Pharmaceutical Ingredient (API) Hydrates as Determined by NMR Relaxation Times	*J Pharm. Sci.*,		in press	2008
Maitani Y., Aso Y., Yamada A., Yoshioka S	Effect of sugars on storage stability of lyophilized liposome/DNA complexes with high transfection efficiency	*Int. J. Pharm.*,		in press.	2008
吉岡澄江、阿曽幸男、川西徹	水分吸着曲線の解析による局方収載添加剤の吸湿性に関する研究 II	医薬品研究	**39**	51-56.	2008
Yoshioka S., Miyazaki T., Aso Y., Kawanishi T	Significance of Local Mobility in Aggregation of b-Galactosidase Lyophilized with Trehalose, Sucrose or Stachyose	*Pharm. Res.*	**24**	1660-1667	2007
吉岡澄江、阿曽幸男、川西徹	水分吸着曲線の解析による局方収載添加剤の吸湿性に関する研究 I	医薬品研究	**38**	228-234	2007
Yoshioka S., Aso Y.	Correlations between Molecular Mobility and Chemical Stability During Storage of Amorphous Pharmaceuticals.	*J. Pharm. Sci.*	**96**	960-981	2007
Miyazaki T., Yoshioka S., Aso, Y., Kawanishi T.	Crystallization rate of amorphous nifedipine analogues unrelated to the glass transition temperature.	*Int. J. Pharm.*	**336**	191-195	2007

Aso Y., Yoshioka S., Miyazaki T., Kawanishi T., Tanaka K., Kitamura S., Takakura A., Hayashi T., Muranushi N.	Miscibility of nifedipine and hydrophilic polymers as measured by ^{1}H-NMR spin-lattice relaxation.	*Chem. Pharm. Bull.*	**55**	1227-1231	2007
A. Hayama, T. Yamamoto, M. Yokoyama, K. Kawano, Y. Hattori, Y. Maitani	Polymeric micelles modified by folate-PEG-lipid for targeted drug delivery to cancer cells in vitro.	*J. Nanosci. Nanotechnol*	**8**	1-6	2007
M. Furuhata, R. Danev, K. Nagayama, Y. Yamada, H. Kawakami, K. Toma, Y. Hattori, Y. Maitani.	Decaarginine-PEG-artificial lipid/DNA complex for gene delivery: nanostructure and transfection efficiency.	*J. Nanosci. Nanotechnol*	**8**	1-8	2008
N. Takahashi, Y. Watanabe, Y. Maitani, T. Yamauchi, K. Higashiyama, T. Ohba.	p-odecylaminophenol derived from the synthetic retinoid, fenretinide: Antitumor efficacy in vitro and in vivo against human prostate cancer and mechanism of action.	*Int. J. Cancer*	**122**	689-698	2008
H.L .Ma, X.R. Qi, W.X. Ding, Y. Maitani, T. Nagai.	Magnetic targeting after femoral artery administration and biocompatibility assessment of superparamagnetic iron oxide nanoparticles.	*J. Biomed. Mater. Res. A.*	**84**	598-606	2007
W. Ding, Y. Hattori, Y. Maitani.	Hydroxyethylated cationic cholesterol derivatives in liposome vectors promote gene expression in the lung.	*Int. J. Pharm*		in ress	2008

M. Fukushima, Y. Hattori, H. Tsukada, K. Koga, E. Kajiwara, K. Kawano, T. Kobayashi, K. Kamata, Y. Maitani.	Adiponectin gene therapy of streptozotocin-induced diabetic mice using hydrodynamic injection.	*J. Gene Med.*	**9**	976-985	2007
Y. Hattori, Y. Maitani.	Low-molecular-weight polyethylenimine enhanced gene transfer by cationic cholesterol-based nanoparticle vector.	*Biol. Pharm. Bull*	**30**	1773-1778	2007
Y. Maitani, S. Igarashi, M. Sato, Y. Hattori.	Cationic liposome (DC-Chol/DOPE=1:2) and a modified ethanol injection method to prepare liposomes, increased gene expression.	*Int. J. Pharm.*	**342**	33-39	2007
Y. Hattori, W. Ding, Y. Maitani.	Highly efficient cationic hydroxyethylated cholesterol-based nanoparticle-mediated gene transfer in vivo and in vitro in prostate carcinoma PC-3 cells.	*J. Control. Release*	**120**	122-130	2007
E. Kajiwara, K. Kawano, Y. Hattori, M. Fukushima, K. Hayashi, Y. Maitani.	Long-circulating liposome-encapsulated ganciclovir enhances the efficacy of HSV-TK suicide gene therapy.	*J. Control. Release*	**120**	104-110	2007

Y. Hattori, M. Fukushima and Y. Maitani.	Non-viral delivery of connexin 43 gene with histone deacetylase inhibitor to human nasopharyngeal tumor cells enhances gene expression and inhibits in vivo tumor growth, , :	*Int. J. Oncol.*	**30**	1427- 1439	2007
Y. Zhang, X. R. Qi, Y. Gao, L. Wei. Y. Maitani, T. Nagai.	Mechanisms of co-modified liver-targeting liposomes as gene delivery carriers based on cellular uptake and antigens inhibition effect.	*J. Control. Release,*	**117**	281-290	2007
Y. Hattori and Y. Maitani,	DNA/lipid complex incorporated with fibronectin to cell adhesion enhances transfection efficiency in prostate cancer cells and xenografts.	*Biol. Pharm. Bull*	**30**	603-607	2007
M. Fukushima, Y. Hattori, T. Yoshizawa, Y. Maitani.	Combination of non-viral connexin 43 gene therapy and docetaxel inhibits the growth of human prostate cancer in mice..	*International Journal of Oncology*	**30**	225-231	2007

研究成果の刊行物・別刷

JPS-07-622.R1(21294)

Wide-Ranging Molecular Mobilities of Water in Active Pharmaceutical Ingredient (API) Hydrates as Determined by NMR Relaxation Times

SUMIE YOSHIOKA, YUKIO ASO, TSUTOMU OSAKO, TORU KAWANISHI

National Institute of Health Sciences, 1-18-1 Kamiyoga, Setagaya-ku, Tokyo 158-8501, Japan

Received 10 October 2007; revised 27 November 2007; accepted 28 November 2007

Published online ? ? ? ? in Wiley InterScience (www.interscience.wiley.com). DOI 10.1002/jps.1294&

ABSTRACT: In order to examine the possibility of determining the molecular mobility of hydration water in active pharmaceutical ingredient (API) hydrates by NMR relaxation measurement, spin–spin relaxation and spin–lattice relaxation were measured for the 11 API hydrates listed in the Japanese Pharmacopeia using pulsed ^{1}H-NMR. For hydration water that has relatively high mobility and shows Lorentzian decay, molecular mobility as determined by spin–spin relaxation time (T_2) was correlated with ease of evaporation under both nonisothermal and isothermal conditions, as determined by DSC and water vapor sorption isotherm analysis, respectively. Thus, T_2 may be considered a useful parameter which indicates the molecular mobility of hydration water. In contrast, for hydration water that has low mobility and shows Gaussian decay, T_2 was found not to correlate with ease of evaporation under nonisothermal conditions, which suggests that in this case, the molecular mobility of hydration water was too low to be determined by T_2. A wide range of water mobilities was found among API hydrates, from low mobility that could not be evaluated by NMR relaxation time, such as that of the water molecules in pipemidic acid hydrate, to high mobility that could be evaluated by this method, such as that of the water molecules in ceftazidime hydrate.
 J Pharm Sci 9999:1–11, 2007
Keywords: NMR relaxation time; dynamics; hydrate; DSC; water vapor sorption isotherm

INTRODUCTION

Correlations between chemical stability and molecular mobility have been demonstrated for various amorphous pharmaceuticals in the solid state.[1] Furthermore, the chemical stability of active pharmaceutical ingredient (API) hydrates is suggested to be correlated with the molecular mobility of water of hydration present in the crystalline structure.[2,3]

Water molecules in API hydrates exhibit a variety of physical states,[4,5] suggesting a range of molecular mobilities; water molecules incorporated into rigid crystalline structures may have low molecular mobility, whereas less rigid structures contain water molecules with greater mobility. Hydration water plays an important role in determining the physical characteristics—such as solubility[6] and flowability—of the API hydrate. Therefore, an understanding of the physical properties of hydration water, such as molecular mobility, is critical in the formulation of API hydrates.

The molecular mobility of water in solids may be determined by various methods, such as dielectric relaxation spectroscopy[7] and FT-Raman

Correspondence to: Sumie Yoshioka (Telephone: 81-3-3700-8547; Fax: 81-3-3707-6950; E-mail: yoshioka@nihs.go.jp)

Journal of Pharmaceutical Sciences, Vol. 9999, 1–11 (2007)

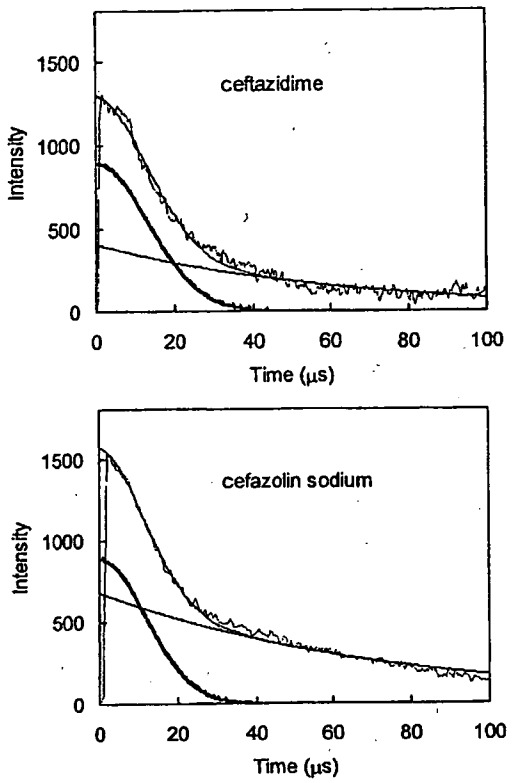

Figure 1. Free induction decay for ceftazidime and cefazolin sodium hydrates.

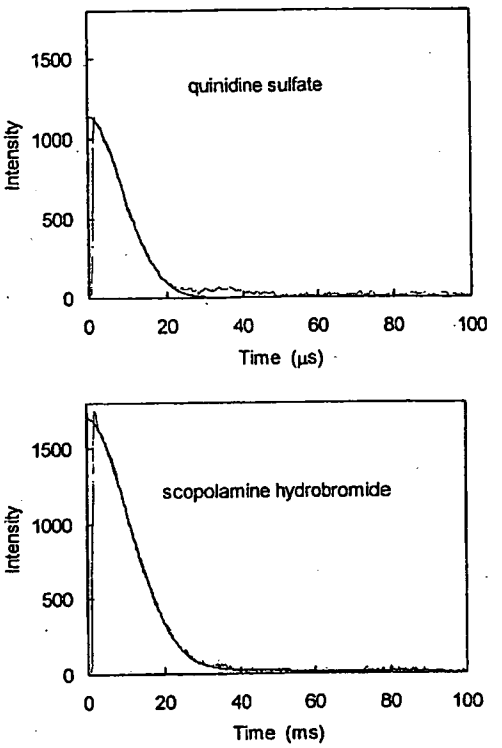

Figure 2. Free induction decay for quinidine sulfate and scopolamine hydrobromide hydrates.

spectroscopy.[8] NMR is also utilized to determine the molecular mobility of water in the solid state,[9] and to examine the various mechanisms by which solids interact with water.[10,11] However, there have been few studies in which the molecular mobility of water in API hydrates was determined using NMR. This may be because ^{1}H-NMR, even high resolution ^{1}H-NMR, cannot separate the peaks of the water protons from those of the protons in other components, which prevents specific determination of water mobility. Although the preparation of API hydrate samples using ^{17}O-labeled water allows to specifically determine the mobility of the water molecules by ^{17}O-NMR, unaffected by the other components, this approach requires high cost and much labor. Thus, determination of the molecular mobility of

Table 1. Water Content of API Hydrates

API Hydrate	Number of H_2O per Molecule Specified in JP	Number of H_2O per Molecule Determined by KF	Spin–Spin Relaxation of H_2O
Cefazolin sodium	5	4.67	Lorentzian
Ceftazidime	5	5.04	Lorentzian
Amoxicillin	3	2.94	Lorentzian
Ampicillin	3	2.96	Lorentzian
Berberine Chloride	Not specified	2.67	Gaussian
Quinine hydrochloride	2	1.31	Gaussian
Scopolamine hydrobromide	3	2.32	Gaussian
Saccharin sodium	2	1.15	Gaussian
Pipemidic acid	3	2.9	Gaussian
Sulpyrine	1	0.98	Gaussian
Quinidine sulfate	2	1.95	Gaussian

DOI 10.1002/jps

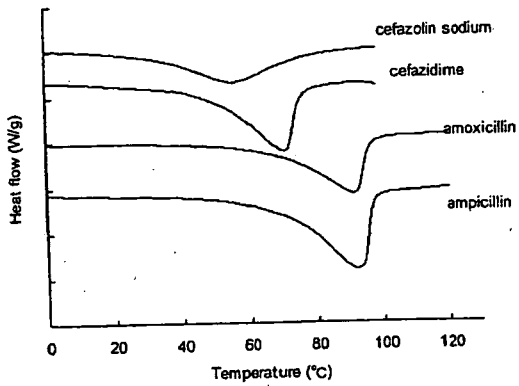

Figure 3. DSC thermograms for four antibiotic hydrates.

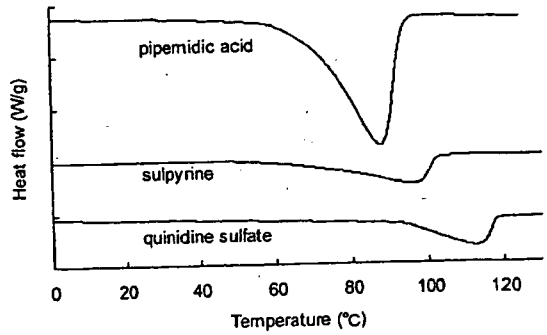

Figure 5. DSC thermograms for API hydrates showing a single endothermic peak.

hydration water in API hydrates using NMR holds some challenges.

However, it is possible to determine the molecular mobility of hydration water in API hydrates by spin–spin relaxation measurement, if the spin–spin relaxation time (T_2) of the water protons is significantly different from that of the API protons. Furthermore, the spin–lattice relaxation time (T_1) of the water protons may be a useful indicator of water mobility, if the ratio of water protons to API protons is sufficiently large, or if the water protons have a correlation time (τ_c) corresponding to the T_1 minimum, such that the T_1 of the water proton is sensitively reflected in the measured T_1 value without being affected by spin diffusion between the water and the API protons. Moreover, even if the ratio of water protons to API protons is not particularly large, and even if water proton does not have a τ_c corresponding to the T_1 minimum, it may be possible to compare the molecular mobility of hydration water in API hydrates based on measured T_1 values, if both of the T_1 of the API proton and the ratio of water protons to API protons are similar for all of the API hydrates compared.

The purpose of this study was to examine the possibility of determining the molecular mobility of hydration water in API hydrates by NMR relaxation measurement. Spin–lattice relaxation, which reflects motions of MHz order, and spin–spin relaxation, which reflects slower motions, were measured for the 11 API hydrates listed in the Japanese Pharmacopeia (JP) using pulsed ^{1}H-NMR, which allows more simplified measurements than high-resolution ^{1}H-NMR. Furthermore, the ease of evaporation of the hydration water was determined under nonisothermal and isothermal conditions using DSC and water vapor sorption isotherm analysis, respectively, and the relationship between the ease of evaporation and the measured values of T_1 and T_2 was examined.

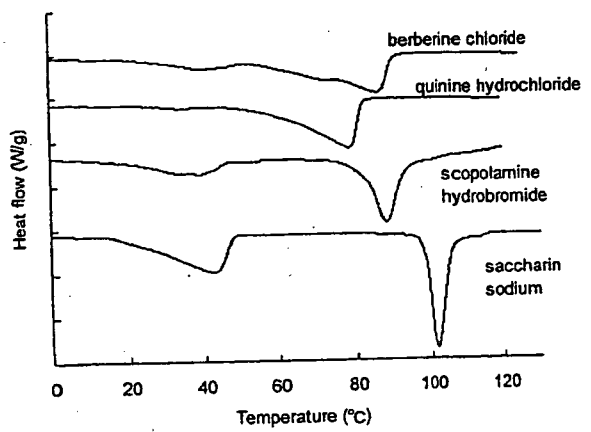

Figure 4. DSC thermograms for API hydrates showing two endothermic peaks.

EXPERIMENTAL

Materials

Cefazolin sodium, ceftazidime, amoxicillin, ampicillin, scopolamine hydrobromide, pipemidic acid, quinidine sulfate hydrates were purchased from Sigma[Q2], and berverine chloride, quinine hydrochloride, saccharin sodium, sulpyrine and disodium hydrogen phosphate 12 H_2O were purchased from Wako[Q3], and di-sodium hydrogen phosphate 2 H_2O was from Merck[Q4].

DOI 10.1002/jps

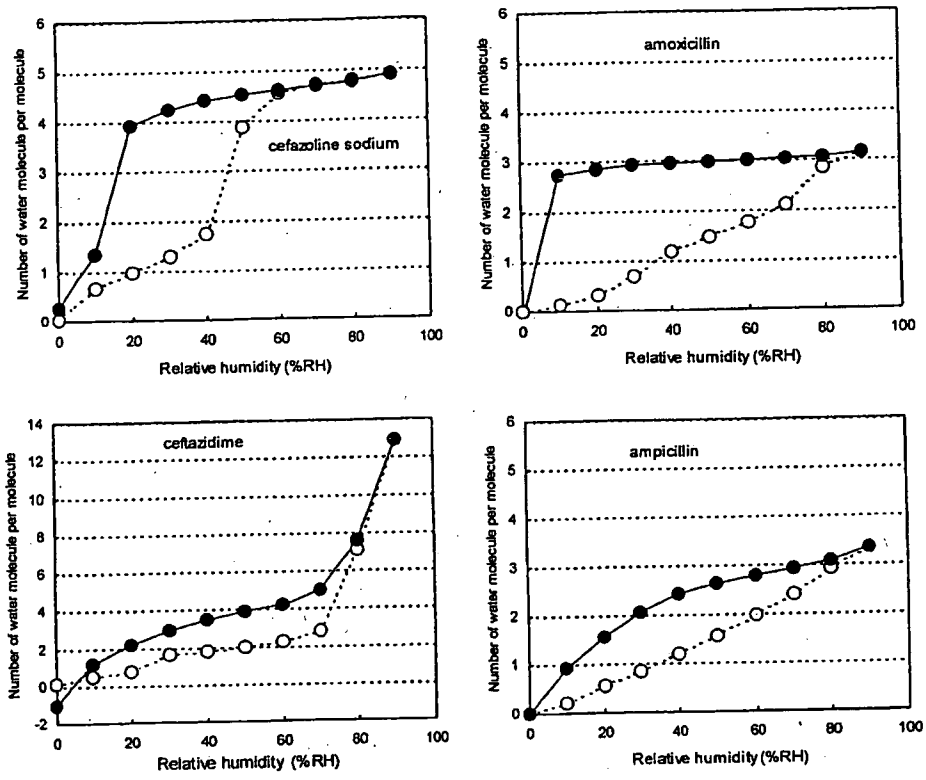

Figure 6. Water sorption isotherms for four antibiotic hydrates.

OK

NMR Relaxation Times

The free induction decay (FID) of protons in API hydrates was obtained using a pulsed NMR spectrometer (25 MHz, JNM-MU25, JEOL Q5, Tokyo, Japan). FID was obtained at 10, 20, 30, and 40°C. The 90° pulses were 2 μs in duration. The "solid echo," with an echo delay of 10 μs, was used in the detection stage of all measurements, in order to overcome the effects of the dead-time.[12] Measurement was repeated four times with a recycling time over five times of the T_1 value measured as described below.

The FID signals obtained between 2.6 and 100 μs that showed only Gaussian-type decay were fitted to Eq. (1) to calculate the T_2 of proton. FID signals obtained for quinidine sulfate and pipemidic acid hydrates showed a small diversion from Gaussian behavior (beat signal) in the final stage of relaxation, suggesting Abragam-type relaxation.[13] However, T_2 was calculated according to Eq. (1) for the purpose of comparison among API hydrates. The FID signals that show both Gaussian and Lorentzian decay patterns were fitted to Eq. (2) representing the summation of the Gaussian and Lorentzian equations.

$$I(t) = I_0 \exp\left[-\left(\frac{t}{T_2}\right)^2\right] \tag{1}$$

$$I(t) = I_0\left[P_G \exp\left(-\left(\frac{t}{T_{2(G)}}\right)^2\right) + P_L \exp\left(-\frac{t}{T_{2(L)}}\right)\right] \tag{2}$$

where $I(t)$ and I_0 are signal intensity at time t and time 0. $T_{2(G)}$ and $T_{2(L)}$ are T_2 for Gaussian decay and Lorentzian decay, respectively, and P_G and P_L are the proportion of protons that show Gaussian decay and Lorentzian decay, respectively.

The T_1 of proton in API hydrates was determined at 30°C by the inversion recovery method. T_1 was calculated according to Eq. (3).

$$I(t) = I_0\left(1 - 2\exp\left(-\frac{t}{T_1}\right)\right) \tag{3}$$

DOI 10.1002/jps

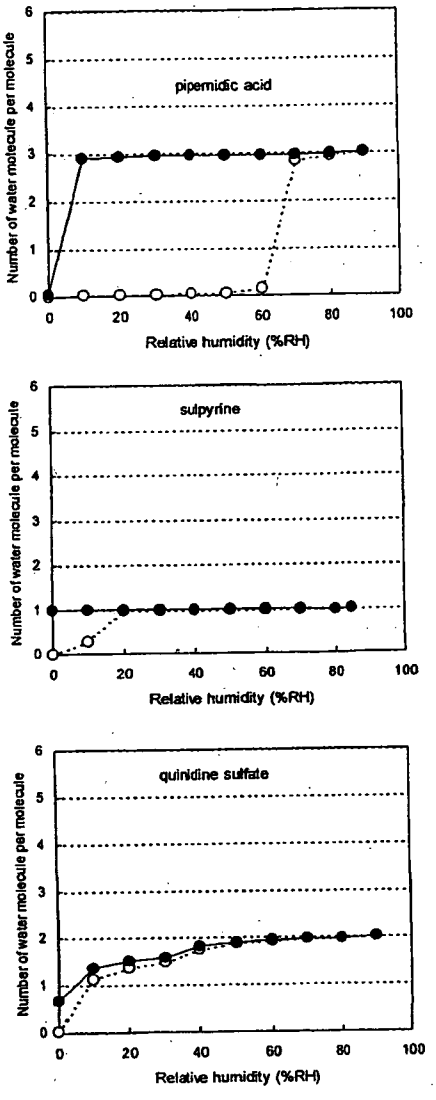

Figure 7. Water sorption isotherms for API hydrates showing a single endothermic peak in DSC thermogram.

Differential Scanning Calorimetry (DSC)

Modulated temperature DSC experiments were performed using a commercial system (2920; TA Instruments[Q6], DE) attached to a refrigerated cooling accessory. The conditions were as follows: modulation period of 100 s, a modulation amplitude of ±0.5°C, and an underlying heating rate of 1°C/min. Temperature calibration was performed using indium. Samples (approximately 10 mg) were put in a pan without a lid. Nitrogen gas was flowed at 30 mL/min.

Water Sorption Isotherm

Water sorption isotherms were measured gravimetrically at 25°C using the automated sorption analyzer from VTI Corp[Q7]. (FL). Prior to water sorption and desorption, samples were dried at 60°C and reduced pressure, until the partial vapor pressure became less than 0.0. Equilibrium water content was measured at ascending partial vapor pressures ranging from 0.10 to 0.95, then at descending partial vapor pressures ranging from 0.95 to 0.00 in steps of 0.10 or 0.05. Equilibrium was regarded to have been achieved once the change in sample weight was less than 0.001 mg over 10 min. The limit duration for measurement at a partial vapor pressure was 10 h for scopolamine hydrobromide and 5 h for the others.

RESULTS

NMR Relaxation Times

Figures 1 and 2 show representative examples of the time courses of spin–spin relaxation observed for the 11 API hydrates. Of the four antibiotic hydrates, all exhibited both Gaussian-type decay and Lorentzian decay, as exemplified by ceftazidime and cefazolin sodium hydrates (Fig. 1). The other seven API hydrates exhibited only Gaussian-type decay, as exemplified by quinidine sulfate and scopolamine hydrobromide hydrates (Fig. 2).

In order to calculate the proportion of water protons to API protons, which is required to obtain the T_2 of the water protons by curve-fitting of decay patterns, the number of water molecules per API hydrate molecule was measured by the Karl Fischer method. The results are shown in Table 1, in which the values specified in the JP are also noted for the purpose of comparison. The measured water contents were consistent with those specified in the JP for pipemidic acid, sulpyrine, and quinidine sulfate hydrates, as well as all antibiotic hydrates except for cefazolin sodium hydrate. In contrast, quinine hydrochloride, scopolamine hydrobromide, and saccharin sodium hydrates showed smaller water contents than those specified in the JP.

The time courses of spin–spin relaxation showing both Gaussian decay and Lorentzian decay observed for the four antibiotic hydrates were well fitted to Eq. (2) using the proportion of water protons calculated from the measured water

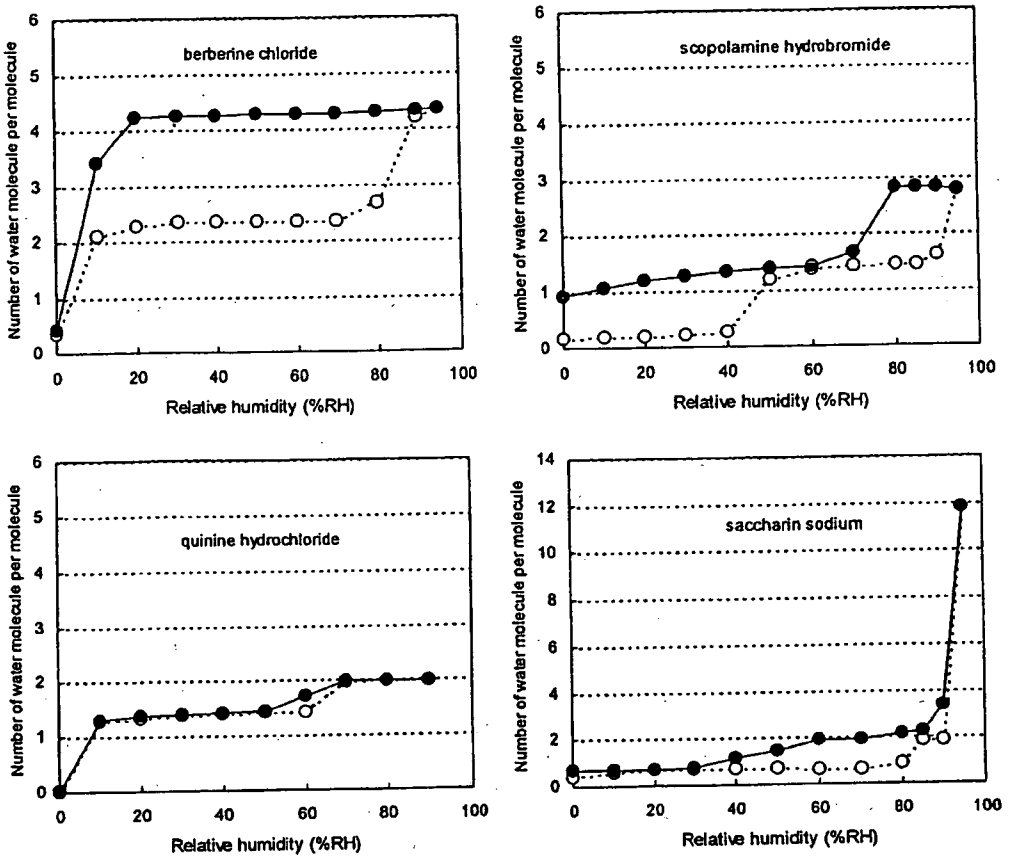

Figure 8. Water sorption isotherms for API hydrates showing two endothermic peaks in DSC thermogram.

content, as shown by the regression curve in Figure 1. Therefore, all of the water protons in the molecule are considered to show Lorentzian decay, and the Gaussian decay is attributed to the drug protons. The T_2 of the Lorentzian decay was calculated according to Eq. (2), and the results will be discussed below. For cefazolin sodium hydrate, better curve-fitting was obtained by regression analysis using a slightly larger value for the proportion of water protons than that calculated from the measured water content. This suggests that a small number of the drug protons exhibit Lorentzian decay; however, it is possible that the water content of the sample used for NMR measurement was different from that of the sample used for Karl Fischer measurements.

The seven API hydrates other than the antibiotic hydrates did not exhibit Lorentzian decay, indicating that all water protons and drug protons in the molecule showed Gaussian decay. The T_2 of the water protons was calculated according to Eq. (1), assuming that the T_2 of the drug protons is similar to that of the water protons. The results will be discussed below.

DSC Thermograms

Figures 3–5 show DSC thermograms measured for the 11 API hydrates. The four antibiotic hydrates, which exhibited Lorentzian decay upon spin–spin relaxation, showed a single endothermic peak due to water evaporation, as shown in Figure 3. In contrast, the API hydrates that did not exhibit Lorentzian decay showed two endothermic peaks (Fig. 4), or one peak (Fig. 5).

The temperature at which an endothermic peak due to water evaporation is observed may be considered to represent the ease of evaporation of hydration water under nonisothermal conditions. The onset temperature was determined as a parameter for approximate comparison of ease of evaporation among the API hydrates, along with ease of evaporation under isothermal conditions as

DOI 10.1002/jps

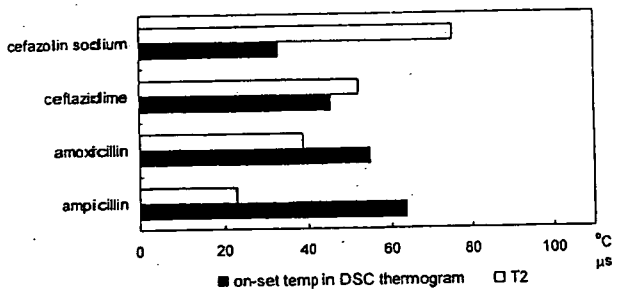

Figure 9. Correlation between onset temperature and T_2 for four antibiotic hydrates.

determined by water vapor sorption analysis. Onset temperature is known to depend on various factors, such as the heating rate, the shapes of the pan and lid, the surface area of the sample, and the flow rate of nitrogen gas. In this study, controllable factors such as the heating rate and the flow rate of nitrogen gas were kept constant, and a pan without a lid was used. The onset temperatures obtained will be discussed below.

Water Vapor Sorption Isotherm

Figures 6–8 show water sorption isotherms observed for the four antibiotic hydrates, the other three API hydrates that exhibited a single endothermic peak due to water evaporation, and the four API hydrates that exhibited two peaks due to water evaporation, respectively. The y-axis represents the number of water molecules per API hydrate molecule, calculated from the water content measured by the Karl Fischer method, assuming that all water molecules present in the sample were evaporated during the drying process

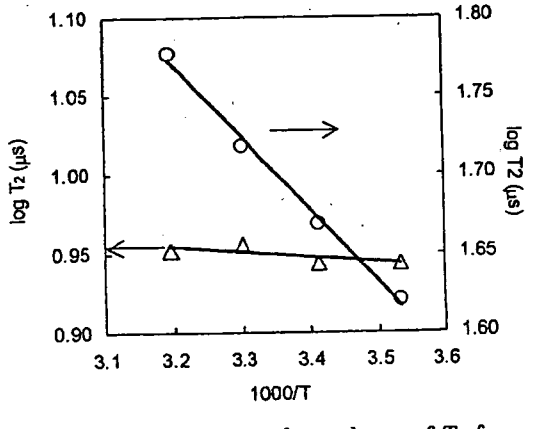

Figure 10. Temperature dependence of T_2 for ceftazidime (circle) and pipemidic acid (triangle) hydrates.

(60°C, reduced pressure) prior to the sorption and desorption processes.

The water sorption isotherms (Fig. 6) observed for the four antibiotic hydrates, which exhibited Lorentzian decay upon spin–spin relaxation, indicate that during the desorption process, the water content decreased with decreasing humidity in the range 90–0% RH, with a significant slope in the water content versus humidity plot.

Among the three API hydrates that did not exhibit Lorentzian decay and showed a single endothermic peak due to water evaporation, pipemidic acid and sulpyrine hydrates gave water desorption isotherms in which the water content was constant over a wide humidity range, as shown in Figure 7. Quinidine sulfate also showed a flat line in the water content versus humidity plot, though it was observed only at high humidities.

The water desorption isotherms observed for the other four API hydrates (except berberine chloride), which did not exhibit Lorentzian decay and showed two endothermic peaks due to water evaporation, indicated that the water content remained approximately constant at two levels (Fig. 8).

DISCUSSION

The molecular mobility of hydration water in API hydrates was found to vary over a wide range; some, such as ceftazidime hydrate, contain hydration water that shows Lorentzian decay upon spin–spin relaxation, while others contain hydration water that shows Gaussian decay.

Hydration Water Showing Lorentzian Decay

All of the water molecules present in the four antibiotic hydrates were found to exhibit Lorentzian decay, because the proportion of Lorentzian decay was consistent with the proportion of water protons calculated from the water content measured by the Karl Fischer method (Fig. 1). The finding that the water molecules in the antibiotic hydrates showed Lorentzian decay rather than Gaussian decay suggests that water molecules are held in voids in the crystal, rather than being firmly trapped in the crystal lattice. These water molecules may evaporate through channels formed in the interior of the crystal.[14] Hydration water that requires more energy to be released

may exhibit a higher onset temperature of the endothermic peak due to water evaporation in DSC.

The T_2 values determined based on Lorentzian decay is related with τ_c by Eq. (4), such that a smaller value of T_2 represents a larger τ_c (lower mobility).

$$\frac{1}{T_2} = \frac{\gamma^4 \hbar^2 I(I+1)}{5r^6}\left(3\tau_c + \frac{5\tau_c}{1+\omega_0^2\tau_c^2} + \frac{2\tau_c}{1+4\omega_0^2\tau_c^2}\right) \quad (4)$$

where γ, ω_0, I, r, and $\hbar$ are the gyromagnetic ratio, resonance frequency, spin quantum number, spin distance, and the Plank's constant divided by 2π.

As shown in Figure 9, T_2 increased as the onset temperature (Fig. 3) decreased, indicating that hydration water which evaporates at lower temperatures has greater molecular mobility as determined by T_2. This correlation between T_2 and the ease of evaporation under nonisothermal conditions may be explained by assuming that hydration water with a greater T_2 (higher mobility) can escape through channels at a lower temperature.

In order to gain further insight into the correlation between ease of evaporation and the molecular mobility of the hydration water, the ease of evaporation under isothermal conditions was evaluated by water sorption isotherm measurement. Each of the four antibiotic hydrates exhibited a desorption isotherm showing decreases in water content associated with decreases in humidity (Fig. 6). As discussed below, the crystal form of ampicillin hydrate appeared to be altered during the drying process prior to the measurement of water sorption isotherms. Therefore, the isotherm obtained for ampicillin could not be compared with the NMR and DSC data. However, such detrimental effect of predrying was not observed for the other three antibiotic hydrates. The negative water content observed after the desorption process for ceftazidime may be due to chemical degradation occurred under high-humidity conditions or incomplete evaporation of hydration water during predrying. Compared to amoxicillin hydrate, cefazolin sodium hydrate, which has a larger T_2 value, exhibited a greater slope in its water content versus humidity plot. Furthermore, cefazolin sodium exhibited rapid dehydration when humidity was decreased below 20% RH, whereas amoxicillin did not exhibit rapid dehydration until humidity was decreased below 10% RH. These findings suggest that the ease of evaporation of hydration water under isothermal conditions is correlated with molecular mobility as determined by T_2, which supports the conclusion obtained based on DSC measurement. For ampicillin, the slope of the water content versus humidity plot was greater than that of amoxicillin hydrate despite its lower molecular mobility as determined by T_2 and higher onset temperature. This suggests that the drying conditions prior to the sorption and desorption processes were inadequate, which may result in destruction of the crystalline structure. Thus, the isotherm obtained for ampicillin could not be compared with the NMR and DSC data.

As exemplified by ceftazidime hydrate (Fig. 10), T_2 increased significantly with increasing temperature, indicating that T_2 reflects the increases in molecular mobility associated with increases in temperature. Thus, molecular mobility can be considered to correlate with T_2. As shown in Figure 11, antibiotic hydrates with smaller T_2

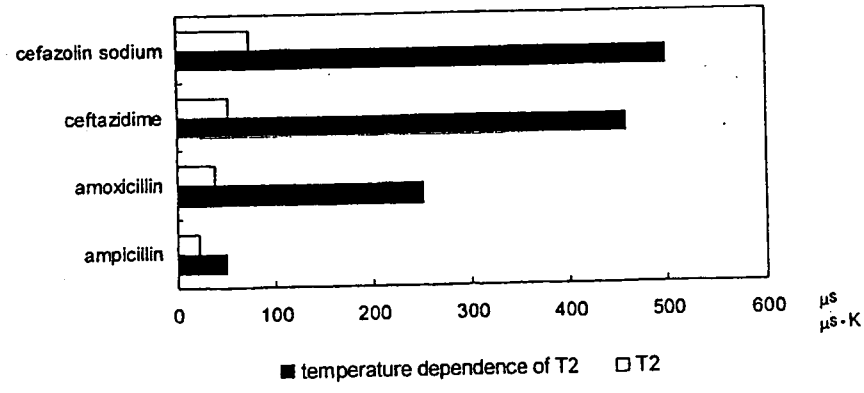

Figure 11. Correlation between T_2 and temperature dependence of T_2 for four antibiotic hydrates.

DOI 10.1002/jps

values showed a smaller change in T_2 with temperature change. This finding suggests that lower values of T_2 reflect a smaller scale of molecular motion, with lower activation energies.

Spin–lattice relaxation time (T_1) is known to reflect molecular mobility, similarly to T_2, but increases with decreasing T_2 (with decreasing molecular mobility) in the slow motional regime. The T_1 values of water protons in the presence of drug protons cannot be determined due to spin diffusion, but an approximate determination of T_1 for water protons is possible if the proportion of water protons is large. For example, in $Na_2HPO_4 \cdot 12H_2O$ and $Na_2HPO_4 \cdot 2H_2O$, water protons are predominant (24/25 and 4/5, respectively). $Na_2HPO_4 \cdot 12H_2O$ exhibits slower spin–spin relaxation (larger T_2) (Fig. 12), and faster spin–lattice relaxation (smaller T_1) (Fig. 13) compared to $Na_2HPO_4 \cdot 2H_2O$, which indicates that both T_1 and T_2 reflect the molecular mobility of hydration water. For the antibiotic hydrates examined, however, correlations between T_1 and T_2 were not observed, as shown in Figure 14. This finding indicates that for API hydrates containing a significant amount of drug protons, such as antibiotic hydrates, the molecular mobility of the hydration water is not reflected in T_1.

Hydration Water Showing Gaussian Decay

As mentioned previously, all of the API hydrates other than the four antibiotic hydrates exhibited only Gaussian decay (Fig. 2). The value of T_2 did not vary significantly among the API hydrates, as shown in Figure 15. Furthermore, the onset temperatures of the single endothermic peaks

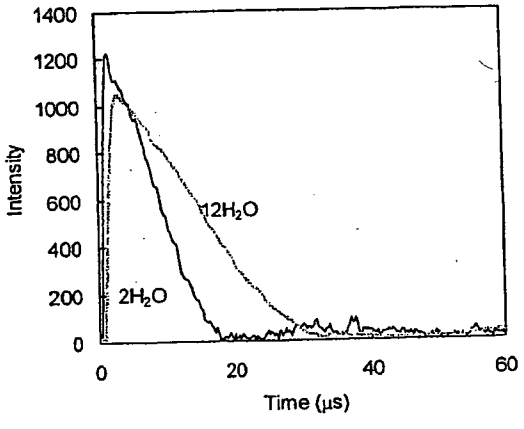

Figure 12. Free induction decay for Na_2HPO_4 $12H_2O$ and $2H_2O$.

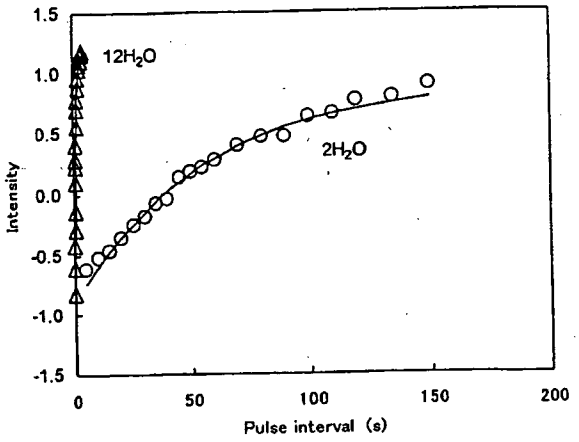

Figure 13. Spin–lattice relaxation for Na_2HPO_4 $12H_2O$ and $2H_2O$.

due to water evaporation for quinidine sulfate, pipemidic acid, and sulpyrine hydrates (Fig. 5), as well as each of the two peaks due to water evaporation observed for quinine hydrochloride, scopolamine hydrobromide, saccharin sodium, and berberine chloride hydrates (Fig. 4), were not correlated with T_2. These findings indicate that the molecular mobility of hydration water that shows Gaussian decay is too low to be reflected in T_2. No correlation between T_2 and molecular mobility is supported by the finding that changes in T_2 associated with changes in temperature were much smaller than those observed for the antibiotic hydrates that exhibited Lorentzian decay, as exemplified by pipemidic acid (Fig. 10). Such low molecular mobility may be attributed to water molecules firmly trapped in the crystal lattice, rather than water molecules trapped in voids in the crystal.

For quinidine sulfate, pipemidic acid, and sulpyrine hydrates, a single endothermic peak was observed in DSC (Fig. 5). The water content versus humidity plots showed a flat line at a certain number of water molecules. Pipemidic acid and sulpyrine showed a flat line at three and one water molecule(s) per hydrate, respectively, and evaporation of these water molecules was observed only under very low humidity (Fig. 7). These findings indicate that water molecules are firmly trapped in the crystal.

For quinine hydrochloride, scopolamine hydrobromide, saccharin sodium, and berberine chloride hydrates, two endothermic peaks were shown in DSC (Fig. 4). The water content versus humidity plots for these hydrates (except for berberine chloride) showed flat lines at two levels

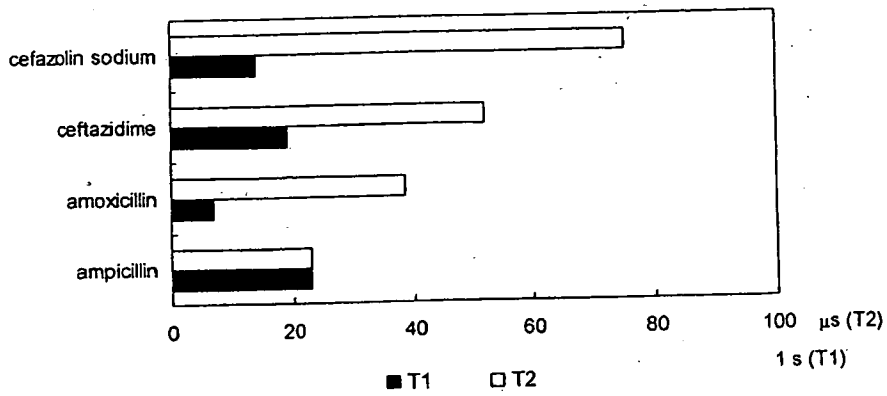

Figure 14. Correlation between T_1 and T_2 for four antibiotic hydrates.

of water content (Fig. 8), suggesting the presence of two water populations: molecules that evaporate at high humidity, and others that evaporate at lower humidity (below 10% RH). This seems to be consistent with the observation of two endothermic peaks in DSC. The endothermic peak observed at a high temperature and the flat line observed at a low humidity may be attributable to hydration water with strong hydrogen–bonding interactions, while the one observed at a lower temperature and higher humidity may be attributable to hydration water with week interactions. The presence of hydration water with week interactions is also supported by the finding that the water contents as measured by the Karl Fischer method were smaller than those specified in the JP (Tab. 1).

CONCLUSION

It was found that spin–spin relaxation time, T_2, is a useful parameter that can indicate the molecular mobility of water of hydration which has relatively high mobility and shows Lorentzian decay upon spin–spin relaxation. For these water molecules, molecular mobility as determined by T_2 is correlated with ease of evaporation both under nonisothermal and isothermal conditions,

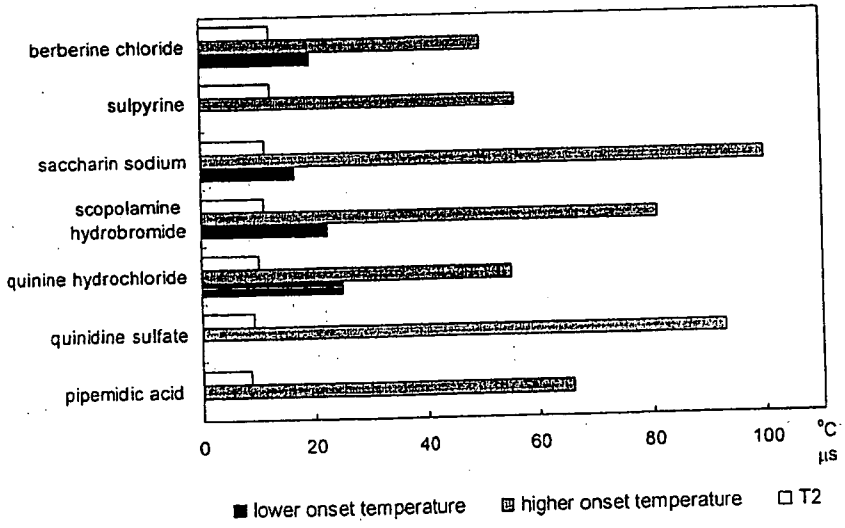

Figure 15. Correlation between onset temperature and T_2 for API hydrates that show Gaussian decay.

DOI 10.1002/jps